ISSN: 2155-9864
Journal of Blood Disorders & Transfusion

OPEN ACCESS Freely available online

Research Article

Morphological Characteristics of Echinocytes: Novel Quantification of Spicule Geometry Using Scanning Electron Microscopy

Samantha Weber-Fishkin[1], Anna Eligulashvili[2], Lesley D Frame[2], Mary D Frame[1*]

[1]Department of Biomedical Engineering, Stony Brook University, Stony Brook, NY, USA; [2]Department of Materials Science and Engineering, University of Connecticut, Storrs, CT, USA

ABSTRACT

Healthy Red Blood Cells (RBCs) are biconcave discs, whose shape is mediated by the components of the erythroid membrane. Pathologic conditions that alter the fluidity of the membrane bilayer result in less deformable cells and, often, abnormal morphologies. Echinocytes are one such morphology characterized by dispersed spicules on the RBC surface. Our objectives are (1) to quantify the well-established qualitative descriptions of stage I, II, and III echinocytes, (2) to determine whether spicule size and symmetry are maintained within a stage of echinocytes, and (3) to determine whether disrupting specific cytoskeletal and transmembrane proteins will result in specific spicule morphologies in cold stored blood. RBCs obtained from healthy human donors were analyzed using optical brightfield and Scanning Electron Microscopy (SEM) imaging. Topology and topography measurements were made for characteristic spicules of RBCs treated with actin-destabilizing agents or agents that weakened the connection between the cytoskeleton and the membrane. Although topologic and topographic measurements within the clinical scoring of RBC morphology match, within each stage of echinocytes, there is non-uniform spicule arrangement and morphology. We show that spicule formation follows five, six or seven-fold symmetry, dependent on temperature, oxygen, and membrane or cytoskeleton stability.

Keywords: Actin; Band 3 protein; Echinocytes; Erythrocytes; Spicules

INTRODUCTION

Healthy human Red Blood Cells (RBCs) are enucleated, contain no mitochondria, and exhibit a biconcave shape with a central pallor, also known as a discocyte. Average RBC dimensions are 7.5 μm-8.7 μm and 1.7 μm-2.6 μm in diameter and thickness, respectively, requiring the ability to deform in order to circulate through capillaries with smaller dimensions [1,2]. While healthy human RBCs are extremely deformable, there are many factors that can alter deformability, resulting in RBC elimination from circulation, blood clotting and disorders [2,3]. RBC deformability is highly dependent on the Surface area to Volume (S/V) ratio, with a typical S/V ratio of 1.5 [3]. A decrease in S/V ratio results in decreased deformability, which correlates well with several pathological disease states including hereditary spherocytosis, hemolytic anemia, and malaria-infected RBCs [3]. RBC deformability is also dependent on hemoglobin concentration, osmotic concentrations, calcium, nitric oxide, alteration of membrane proteins or lipids, aging, temperature, oxygenation, and pH [3,2,4]. Alterations to the concentrations of these regulators result in changes in volume, cellular rigidity, hemolysis, and cell shape [3]. Some disease states, including diabetes, thermal burn injury, coronary artery disease, stroke, and COVID-19, can also alter the properties of the RBC thereby affecting their deformability as they become more rigid and prothrombotic [2,5-10].

Correspondence to: Mary D Frame, Department of Biomedical Engineering, Stony Brook University, Stony Brook, NY, USA, E-mail: mary.frame@stonybrook.edu

Received: 03-Aug-2022, Manuscript No. JBDT-22-17649; **Editor assigned:** 05-Aug-2022, Pre QC No. JBDT-22-17649 (PQ); **Reviewed:** 22-Aug-2022, QC No. JBDT-22-17649; **Revised:** 30-Aug-2022, Manuscript No. JBDT-22-17649 (R); **Published:** 07-Sep-2022, DOI: 10.4172/2155-9864.22.13.518

Citation: Frame MD, Weber-Fishkin S, Eligulashvili A, Frame LD (2022) Morphological Characteristics of Echinocytes: Novel Quantification of Spicule Geometry Using Scanning Electron Microscopy. J Blood Disord Transfus.13:518

Copyright: © 2022 Frame MD, et al. This is an open-access article distributed under the terms of the Creative Commons Attribution License, which permits unrestricted use, distribution, and reproduction in any medium, provided the original author and source are credited.

While it is unknown why RBCs exhibit the discocyte shape, it is postulated that the discocyte shape is related to a RBCs high surface-to-volume ratio and flexibility of the membrane [11]. Several hypotheses exist for how an RBC maintains its erythroid shape, including elastic forces within the membrane, membrane fluidity, electrical forces on the membrane surface, and osmotic or hydrostatic pressures [11,12]. Other theories account for the biconcave shape as an evolution that occurred due to the need to maximize laminar flow within the vasculature [13]. More recently, it was shown that non-muscle myosin controls interactions with the spectrin-actin cytoskeletal meshwork, thereby governing RBC shape and deformability [14]. Regardless of the theory, all hypotheses agree that the biconcave shape is mediated by components of the erythroid membrane, and when the membrane is altered, as in several pathologic conditions, varying RBC morphologies are produced.

Echinocytes are caused by decreased fluidity of the membrane due to an increased membrane lipid concentration, resulting in an abnormal cell contour and deformability [15]. Echinocytes are characterized by a change in RBC shape in which the cell becomes spiculated with distributed points over the entire membrane surface [16,17]. Echinocytes are further divided into three stages by the Bessis' nomenclature; stage I, which is characterized by irregularity of edges, stage II, characterized by spicules in a flat cell, and stage III, characterized by spicules uniformly distributed over the surface of a round cell [18].

The RBC cytoskeleton is composed of an actin-spectrin meshwork connected to the lipid bilayer through a network of proteins anchored to band 3, the main integral membrane protein [19-27]. Spicule formation is induced by an expansion of the lipid bilayer outer leaflet relative to the inner leaflet in which bumps (spicule nucleation sites) form on the membrane surface to accommodate this expansion [28,29]. However, the components of such formed spicules are presently unknown. Current models of spicule formation focus on the membrane bilayer and often overlook the potential contribution of the actin-cytoskeleton. Recent literature suggest the importance of actin in echinocyte formation, as actin reorganization to a box-like arrangement at the rim of the cell is observed in fluorescent confocal images [30].

Actin is a well-conserved structural protein in erythrocytes in which the erythrocyte morphology and adhesion are highly dependent on the actin organization [31]. There has been a widespread assumption that erythrocyte actin filaments are static; however, recent literature reveal the dynamic nature of such filaments in which assembly and reorganization of the actin cytoskeleton are controlled through polymerization and depolymerization by actin binding proteins [32,33]. Any perturbation in the balance between Filamentous (F) and Globular (G) actin states (or their attachment to the membrane) has the potential to alter cell surface contours and cell shape [14,34,35].

Despite the well-known classification of the various stages of echinocytes, there is a paucity in the quantification of spicule geometry to validate these qualitative descriptions. Recent literature models spicule shape for various membrane curvatures and lipid bilayer organization [36]. In this model, spicules are assumed to be axisymmetric, in which individual spicules are joined to the central body along the same axis. The model produces spicule shapes ranging from those with an even width throughout and to a narrower spicule with a wider head and narrower neck. Unfortunately, the cytoskeletal stretching ratio is not yet known for RBCs, and thus this model has limited accuracy. It is thus important to understand the role of the cytoskeleton in producing echinocyte spicules.

Spicule formation is induced by an expansion of the lipid bilayer outer leaflet relative to the inner leaflet in which bumps (spicule nucleation sites) form on the membrane surface to accommodate this expansion [28,29]. However, the total components of such formed spicules are presently unknown. Franke et al., used radiographic contrast media to promote echinocyte formation and found that band 3 and spectrin were co-localized at the root of the spicule, with band 3 at the tip of the spicule [37]. This finding seems to agree with the composition of Extracellular Vesicles (EV) that bud from echinocyte spicules, containing anion transport proteins (band 3) and cytoskeletal proteins (actin and spectrin) [38]. However, the composition and location of actin within echinocyte spicules is presently unknown, as current models of spicule formation focus on the membrane bilayer and often overlook the potential contribution of the actin-cytoskeleton. Recent literature suggest the importance of actin in echinocyte formation, as actin reorganization to a box-like arrangement at the rim of the cell is observed in fluorescent confocal images [30].

This evidence that suggests the presence of integral membrane protein, band 3, and cytoskeletal proteins, spectrin and actin, in the spicule begs the question of organization. The sub-cellular organization of the membrane skeleton is a quasihexagonal lattice centered around actin filaments [20]. The ankyrin complex has 1 band 3 dimer, whereas the actin junctional complex contains 6 band 3 dimers, but it is likely that these two complexes are in close contact with one another. Spectrin is stretched between a complex of actin, adducin, and band 3, further contributing to the hexagonal orientation [20,39]. Thus, we wanted to evaluate the organization of the spicules that from on the surface of the RBC membrane to determine if their organization aligns with the subcellular organization of the membrane and cytoskeletal proteins. If so, this analysis could provide the key players involved in spicule formation.

It is unknown how this dynamic reorganization contributes to echinocyte formation. As the organization of the RBC membrane is well classified, understanding spicule topography and topology can elucidate the underlying structure of echinocytes (Figure 1). A current obstacle to establishing a mechanistic understanding of dynamic reorganization of RBC membrane and echinocyte formation is rooted in visual analysis methods for RBCs. Conventional analysis of RBC morphological features with light microscopy does not provide resolution necessary for quantifying spicule size and shape. In the present study, Scanning Electron Microscopy (SEM) is used, which allows orders of magnitude higher magnification and clearer depiction of spicules (Figures 1A-1H).

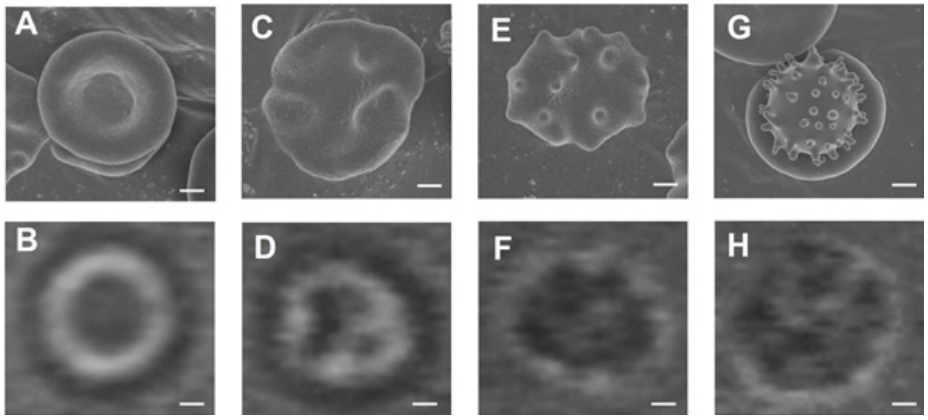

Figure 1: Exemplars of scanning electron microscopy and brightfield images of RBCs. Discocyte (A,B), Stage I Echinocyte (C,D), Stage II Echinocyte (E,F), Stage III Echinocyte (G,H) micrographs obtained *via* FEI Nova NanoSEM 450 FE-SEM (left) paired with micrographs of identical RBC morphologies obtained *via* bright field with XR-Mega 10 ICCD and 60X water-immersion objective (right). Digitized brightfield images brightness and contrast adjusted to 100% using Adobe Photoshop. Scale bars are 1 μm.

In the present study, we hypothesize that spicule morphologies are dependent on temperature, oxygen saturation, and the stability of the erythrocyte membrane and cytoskeleton. The morphology of RBCs exposed to oxygen (de)saturation and elevated temperatures, as in pathologic conditions, i.e., thermal burn injury, and membrane and cytoskeleton disruptors are observed with conventional light microscopy. We then used SEM to capture surface morphological features of the RBCs exposed to the same conditions to quantify the spicule geometries. Lastly, we used cold stored blood in order to quantify these parameters for transfusion ready blood.

MATERIALS AND METHODS

Membrane and cytoskeletal drugs mechanisms of action

Latrunculin A (LatA) has a highly specific mechanism of action in which it sequesters monomeric actin, thereby inhibiting actin polymerization and promoting depolymerization. LatA binds G-actin in a 1:1 nonpolymerizable complex with a Kd of 0.2 μm [31]. Jasplakinolide (Jasp) has the opposite mechanism of action, in which it is a potent inducer of actin polymerization and a stabilizer of actin filaments, with a Kd of 15 nm. Jasp is a commonly known and commercially used small molecule promotor of actin polymerization [40]. Cytochalasin D (CytoD) disrupts the actin cytoskeleton in a non-specific manner in which it stimulates actin polymerization, depolymerization, or redistribution of F-actin without a change in the polymerization state, with a Kd of 2 nm [31,41]. 4'-Diisothiocyano-2, 2'-Stilbene Disulfonic acid (DIDS) is a well-known non-specific inhibitor of band 3, inhibiting the anion exchange of bicarbonate for chloride ions in the RBC, with a Kd of 25.3 nm [42,43].The association of DIDS with band 3 weakens the affinity for ankyrin, resulting in dissociation from the spectrin-actin meshwork [44].

Erythrocyte suspension preparation

Whole blood from healthy human male donors (N=11; 42 ± 16 years; self-identified race/ethnicity: black n=9, Hispanic n=1, Caucasian n=1; ABO type: O+ n=10, A+ n=1) was purchased commercially from BioIVT (Westbury, NY). Whole blood was collected *via* venipuncture (with EDTA) and received cold within 48 hours of collection. Upon receipt, whole blood was immediately centrifuged (5 min, 1600 xg). Platelet Poor Plasma (PPP) was aspirated and saved for later use. Packed erythrocytes (RBC) were washed three times in phosphate buffered saline (PBS, Sigma pH 7.6, 120mmol NaCl, 2.7 mmol KCl, 10 mmol PO_4^{3-}). Packed RBCs and PPP were stored at 4°C and -20°C, respectively, for no more than one week prior to use. RBC washing procedure was repeated each day prior to use; cells were only used if the supernatant remained clear. Erythrocytes were suspended at 50% Hematocrit (Hct) in autologous PPP, in PBS, or incubated with membrane destabilizers in PBS, 2 μm DIDS (30 min, Sigma) or 0.5 μm CytoD (1 hr, Sigma) at 37°C, actin stabilizer, 3.8 μm Jasp (Tocris), or actin destabilizer, 20.9 μm LatA (Tocris) at 37°C for 4 hrs. All drugs were first dissolved in dimethyl sulfoxide (DMSO, Sigma). Suspensions of RBCs in 1% DMSO in PBS were used as a driver (solvent) control. Prism was used to fit a dose response curve to determine the half maximal effective concentration of Jasp and LatA for inducing stage III echinocytes Supplementary Figure 1. The EC50s for Jasp and LatA are on par with what is used previously to sufficiently disrupt actin filaments [19].

Sample Preparation

Morphology: Immediately after drug incubation time, all erythrocyte suspensions were warmed to 37°C or 45°C, while equilibrating with 0% (deoxy) or 10% (saturated) O_2. After 10 minutes, they were mixed to a final concentration of 4% methanol free Paraformaldehyde (PFA, ThermoFisher) in PBS, maintaining oxygen and temperature. After 5 min fixation, RBCs were centrifuged (1600 xg, 2 min), the PFA supernatant discarded, and resuspended in PBS to 1% Hct.

Spicule Geometry: Immediately after drug incubation time, all erythrocyte suspensions were warmed to 37°C or 45°C, while equilibrating with 0% (deoxy) or 10% (saturated) O_2. After 10 minutes, they were mixed to a final concentration of PFA-GA (1.5% PFA-1.5% glutaraldehyde, GA, ThermoFisher), maintaining oxygen and temperature. After 5 min fixation, RBCs were centrifuged (1600 xg, 2 min), the PFA-GA supernatant discarded, and washed 2X in PBS. All suspensions were secondary fixated in 1% OsO_4 for 1 hr and rinsed 3X with DI H_2O for 10 min. The samples were then serially dehydrated with 30, 50, 70, 95, and 100% ethanol for 10 min each and stored in excess 100% ethanol.

Samples were shaken until the pellet was disrupted and cells were uniformly suspended in ethanol. SEM stubs were cleaned in

reagent grade ethanol, and double-sided carbon tape was applied to clean and dry SEM stub. Transfer pipet was used to transfer <5 µl of suspended cells to the carbon tape. Samples were allowed to dry on the carbon tape (ethanol evaporated). A new transfer pipet was used for each sample. Samples were coated with 12 nm-15 nm layer of Au-Pd (~6 nm/min; 2.5 minutes) in Ar with current of 6 mA using a Polaron E5100 sputter coater.

Image Acquisition

Population Morphology: RBC suspensions fixed in PFA (20 µl) were injected into microchannels of fixed height (160 µm) between two glass coverslips separated with carbon nanofiber tape and allowed to settle into a monolayer. Each glass coverslip housed 6 individual microchannels, each with a width of 3-5 mm and length of 20-25 mm, accommodating approximately 20 µl of RBC suspensions. An inverted Nikon Diaphot 200 Microscope with a 60X water immersion objective (Olympus, Numerical Aperture (NA)=1.1) was used to acquire images with an XR-Mega 10 ICCD (Intensified Cooled charge Coupled Device, Solamere Technologies, Inc., Palo Alto, CA).

Spicule Geometry: SEM images were collected using an FEI Nova NanoSEM 450 field emission scanning electron microscope in high vacuum mode. A working distance of 4-5 mm, beam voltage of 2 kV, and the Everhart-Thornley Detector was selected for all images.

Image Analysis

Population morphology: All brightfield images were digitized and analyzed using Fiji [45]. Within Fiji, images were divided by quadrant, of which one was chosen at random for analysis. The cells in each quadrant were analyzed for discocyte, echinocyte (stage I, II, or III), or other morphology. The total number of cells per quadrant were tallied, and the population of each stage of morphology was tabulated. Morphology was scored by clinical standard [18].

Spicule geometry: SEM images at 2,000X – 10,000X magnification were selected for RBC feature analysis. Every image containing cells for SEM image analysis was divided into four quadrants. Within the sample, each measured cell was given an identification code based on its sample number, file name, and quadrant location. Each measured RBC was scored for morphology by clinical standard and with the classifications coined by Brecher and Bessis; normal, echinocyte stage I, echinocyte stage II, or echinocyte stage III [18]. Measurements were made using ImageJ [46]. Before measuring any cell, the scale bar was used to convert from pixels to micrometers to ensure all length measurements were recorded with proper units. Overall dimensions of each measured cell included cell diameter, both the long dimension and the short dimension at 90° to each other. In the case that the thickness of the cell was being measured, the long dimension and the short dimension of the thickness were measured and recorded.

For cells classified as any stage of echinocyte, each spicule was numbered and identified as being an "edge spicule," able to be viewed in profile, or a "face spicule," viewed on the front surface of the cell. Spicule base width, mid-height width, tip width, and height were measured for each edge spicule (Figure 2A).

All further measurements on the given cell were regarding relationships between spicules and their "nearest neighbors." For spicules viewed in profile ("edge spicules"), the nearest neighbor spicules are the two nearest spicules around the circumference of the cell. Distances between edge spicules were measured center to center. For face spicules, nearest neighbors were identified using a concentric circle guide overlain on the image to ensure that spicules within the same plane were compared (Figure 2B). Nearest neighbors for face spicules were defined such that no other spicules lay between them; nearest neighbors were generally within the same plane to ensure the measurement surface is flat and generates an accurate measurement. In the cases where an echinocyte was flat, the nearest neighbors were additionally measured through different concentric circle boundaries.

Additionally, angles between spicules were measured to identify the symmetrical organization of spicules on the RBC surface. In order for an apex spicule to be used for nearest neighbor angle measurement, it must be located on the face of the cell within the innermost circle. If a spicule lies within these constraints but is visually the outermost face spicule, then it cannot be used as the apex of an angle measurement. Once the spicule to be used as the apex of the angle is identified, at least two of that spicule's nearest neighbors must be identified. Angle measurements were taken from one nearest neighbor to the apex spicule, to a different nearest neighbor (Figure 2C). If multiple spicules existed in the innermost circle, each was used as an apex spicule. Angles were recorded for all nearest neighbors surrounding apex spicules. Nearest neighbor spicules were only used for angles if another spicule was not passed when measuring from apex to nearest neighbor.

Statistical analysis

All statistical analyses were performed in Prism 9.3.1 (GraphPad Software). Two-way analysis of variance with Tukey's multiple comparisons test was used to determine differences across temperature, oxygen, and treatment for morphology, height to mid-width ratio, and angles between spicules. One-way analysis of variance with Tukey's multiple comparisons test or Kruskal Wallis with Dunn's multiple comparisons test was used to determine differences in all topology and topography measurements of spicules.

RESULTS

At physiologic temperature (37°C) and arterial oxygen (10%), the population of RBCs in autologous plasma is mostly composed of discocytes, 38.1% ± 27.2 %, followed by stage I echinocytes, 33.8% ± 13.7%, stage III echinocytes, 14.8% ± 17.4%, and stage II echinocytes, 13.3% ± 17.1% (mean ± SD, (Figure 3A). The population of morphologies do not significantly change when oxygen is depleted. However, when temperature is increased to 45°C, both in saturated, arterial, and desaturated oxygen, the population shifts to an increased percentage of echinocytes. This shift in population is more pronounced with high temperature and oxygen depletion (discocytes reduced to 6.2% ± 11.4%); the percentage of stage I echinocytes is unchanged at 35.1% ± 20.6%, and the percentage of stage II and III echinocytes increased to 33.2% ± 15.0% and 25.3% ± 11.0%, respectively. The morphology population of RBCs in PBS does not differ from RBCs in plasma except at 37°C and 0% O_2, in which the population of discocytes of RBCs in PBS, 37.7% ± 16.9%, is less than that of RBCs in plasma, 51.9% ± 26.2%. DMSO maintains the population of discocytes, stage I echinocytes and stage II echinocytes compared to PBS for all temperatures and oxygens. However, DMSO increases the population of stage III echinocytes at 37°C in 10% O_2 and 45°C in 0% O_2 (Figure 3A-3D).

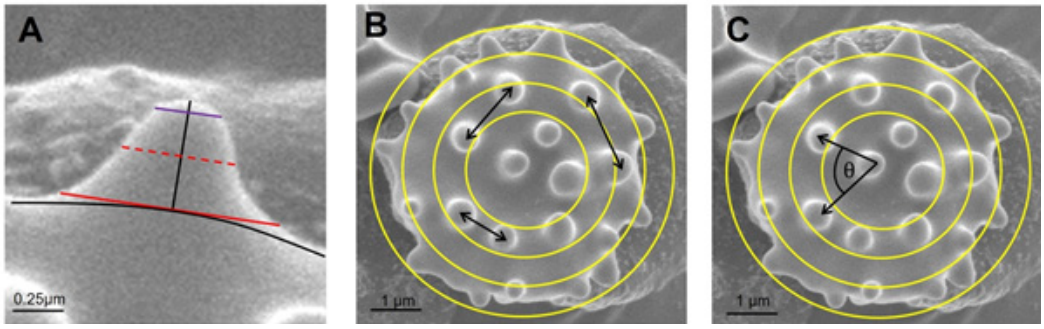

Figure 2: Analysis of echinocyte spicules. (A) Base Width (solid red), mid-width (dotted red), Tip-width (solid purple), and height (solid black line) of an edge spicule. Base width determined *via* asymptote to fitted spicule base arch (solid black curve). (B) Nearest neighbor distances between face spicules within the same plane, identified using an overlain concentric circle guide. (C) Angle between apex spicule to two nearest neighbors.

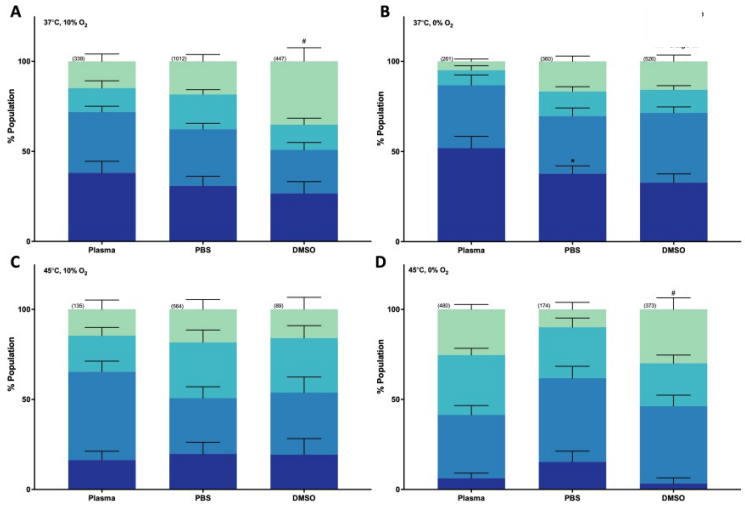

Figure 3: Morphological distribution of RBCs. Population of discocytes, stage I-III echinocytes in autologous plasma alone, PBS alone, and 1%DMSO in PBS (driver control). RBCs in all treatments exposed to typical physiologic temperature (37˚C) (A-B), arterial oxygen saturation (10%O_2) (B,D), deoxygenated (0%O_2) (A,C), and elevated temperature (45˚C) (C,D). Morphology in brightfield micrographs manually scored per clinical standard. Bar graphs indicate mean percentage of the population for each morphology with N=total number of cells scored for morphology, error bars indicate standard error of the mean. (2-way analysis of variance with Tukey's multiple comparisons test, **Note:** *p<0.05 PBS compared to plasma in same conditions, #p<0.05 PBS+1% DMSO compared to PBS in same conditions). **Note:** (■) Discocycle; (■) Stage I; (■) Stage II; (■) Stage III.

Regardless of oxygen, when RBCs at 37˚C are treated with membrane-disruptor, DIDS, or cytoskeleton-disruptors, CytoD, Jasp, or LatA, the population of RBCs shifts to more echinocytes and fewer discocytes (Figures 4A-4B). At physiologic temperature and arterial oxygen, CytoD results in more stage I echinocytes (60.9% ± 8.1%) (Figure 4A). With oxygen depletion (Figure 4B), LatA shifts the population of RBCs from discocytes to stage II echinocytes. DIDS conversely shifts the population from discocytes to primarily stage III echinocytes. Similarly, RBCs treated with DIDS in elevated temperature and arterial oxygen, also experience a population shift from discocytes to far more stage III echinocytes (Figure 4C). However, in high temperature and oxygen depletion, DIDS shifts the morphology away from stage III echinocytes, with an increase in stage I echinocytes instead (Figure 4D). At 45˚C, the morphological distribution of CytoD, Jasp, and LatA were not different than PBS+1% DMSO (Figures 4C and 4D).

Overall, it was noted that temperature, oxygen, and treatment influence the observed population of RBC morphologies. In some instances, however, temperature, oxygen, or treatment had no statistically significant effect on the morphology. To determine whether the size of the RBC, the topology, and/or topography of the echinocyte spicules are affected by temperature, oxygen, and treatment, the SEM images of RBCs were evaluated.

The diameters of RBCs were determined based on the longest observable width of each measured cell. For cells with spicules present, the diameter was measured for the longest width of the cell, excluding the spicule. Across all conditions, the sizes of RBCs decreased from discocyte through the echinocyte stages. Discocytes and stage I echinocytes are similar in size, with a diameter of 6.1 ± 0.5 µm and 6.1 ± 0.7 µm, respectively. Stage II and stage III echinocytes are both reduced size, with average diameter of 5.7 ± 0.7 µm and 5.4 ± 0.8 µm, respectively (Figure 5A). Diameters of RBCs in PBS and PBS + 1% DMSO did not differ from the diameters of RBCs in plasma (Figure 5B). Treatment does not appear to significantly affect the size of discocytes or stage II echinocytes. CytoD, however, increases the diameter of stage I and stage III echinocytes from 5.7 ± 0.6 µm in PBS+1% DMSO to 6.5 ± 0.6 µm and from 5.0 ± 0.6 to 6.1 ± 0.6, respectively. Jasp and DIDS both induce smaller stage I echinocytes than CytoD (Figure 5B).

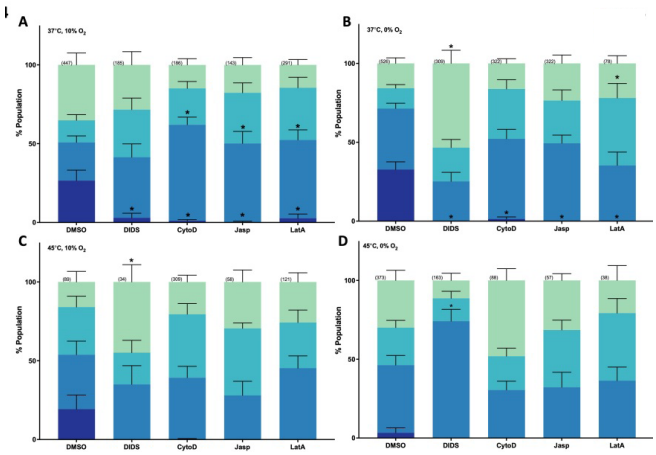

Figure 4: Morphological distribution of RBCs with membrane- or cytoskeleton-destabilizing treatments. Population of discocytes, stage I-III echinocytes in 1%DMSO in PBS (driver control), membrane destabilizer (DIDS, 2 μm), or actin disruptors (CytoD 0.5 μm, Jasp 3.8 μm, or LatA 20.9 μm). All RBCs treated with pharmacologic agent are in PBS with 1%DMSO. RBCs in all treatments exposed to typical physiologic temperature (37˚C) (A-B), arterial oxygen saturation (10%O_2) (B,D), deoxygenated (0%O_2) (A,C), and elevated temperature (45˚C) (C,D). Morphology in brightfield micrographs manually scored per clinical standard. Bar graphs indicate mean percentage of the population for each morphology with N=total number of cells scored for morphology, error bars indicate standard error of the mean. (2-way analysis of variance with Tukey's multiple comparisons test, **Note:** *p<0.05 compared to PBS+1%DMSO in same conditions). (■) Discocycle; (■) Stage I; (■) Stage II; (■) Stage III.

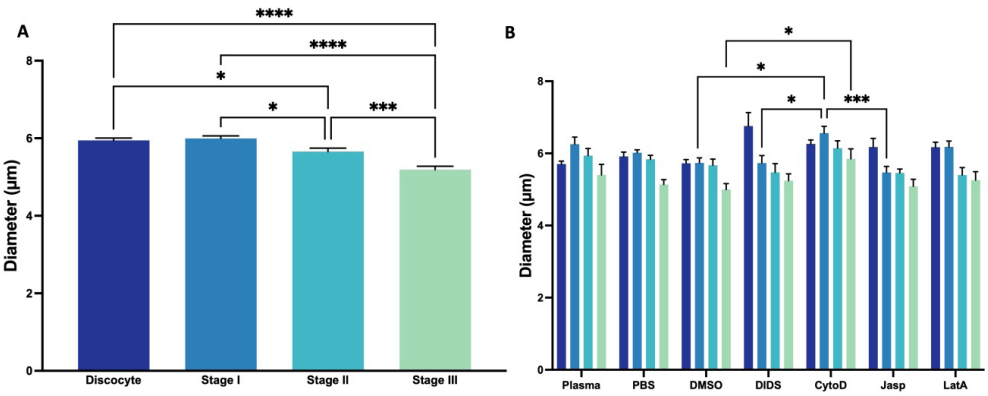

Figure 5: Size (long diameter) of discocytes and echinocytes from FE-SEM micrographs. Long diameter for discocytes and echinocytes from manual scoring by clinical standard of FE-SEM micrographs. (A) Diameter of discoctyes, stage I-III echinocytes of RBCs, regardless of treatment. Bar graphs indicate mean diameter, error bars indicate standard error of the mean. Kruskal Wallis with Dunn's multiple comparison, **Note:** *p<0.05, ***<0.001, ****<0.0001. (B) Diameter of discocytes, stage I, II, or III echinocytes in autologous plasma, PBS, DMSO (driver control), or with membrane destabilizer (DIDS) or actin-disruptors (CytoD, Jasp, LatA). Bar graphs indicate mean diameter, error bars indicate standard error of the mean. 2-way analysis of variance with Tukey's multiple comparisons test, *p<0.05, ***<0.001 compared to other treatments for the same morphology. **Note:** (■) Discocycle; (■) Stage I; (■) Stage II; (■) Stage III.

The topology and topography of RBCs were evaluated through comparison of the global base-width (Figure 6A), mid-width (Figure 6B), tip-width (Figure 6C), and height (Figure 6D) for edge spicules. Spicules get progressively narrower and taller from stage I through III echinocytes. The distance between nearest neighbors of both face and edge spicules and the angle between face spicules gets progressively smaller from stage I through III echinocytes (Figures 6E and 6F). The trends shown in Figure 5 of increased density of tall and narrow spicules from stage I to II to III was apparent regardless of oxygen saturation or temperature treatment.

Spicule shape was normalized by examining the ratio of spicule height to the width at half height (mid-width). Such a comparison illustrates the tall narrow nature of stage III spicules and the short wide shape of stage I spicules without obfuscation due to absolute dimensions. Comparison of Height to Mid-width (H/MW) ratio to the absolute width at the base and the mid-width for stage I, II, and III echinocytes shows that stage I echinocyte spicules tend to have a lower aspect ratio (i.e., they are short and wide) and there is a greater difference between the width of the spicule at the base compared to the width at half-height. In addition, not only do stage III spicules have a higher aspect ratio shape, the overall width is less and the difference between the width at the base and width at mid-height is less pronounced. The H/MW ratio resents the shape of the spicule. Stage I echinocytes have a small H/MW ratio, representing a broad, short spicule, whereas stage III echinocytes have a large H/MW ratio, representing a narrow, tall spicule. Stage II spicules' H/MW ratio falls between that of stage I and III (Figures 7A-7E).

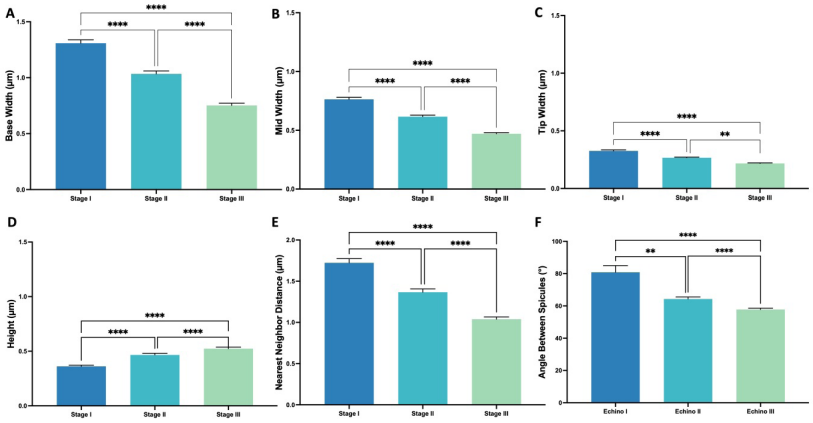

Figure 6: Geometry of echinocyte spicules from FE-SEM micrographs. (A) Base Width of edge spicules. (B) Mid Width of edge spicules. (C) Tip Width of edge spicules. (D) Height of edge spicules. (E) Nearest neighbor distance of edge spicules or face spicules within the same plane. (F) Angle between apex spicule and two nearest neighbor spicules. Bar graphs indicate mean, error bars indicate standard error of the mean. Kruskal Wallis with Dunn's multiple comparison, **Note:** **p<0.01, ****<0.0001. (■) Discocycle; (■) Stage I; (■) Stage II; (■) Stage III.

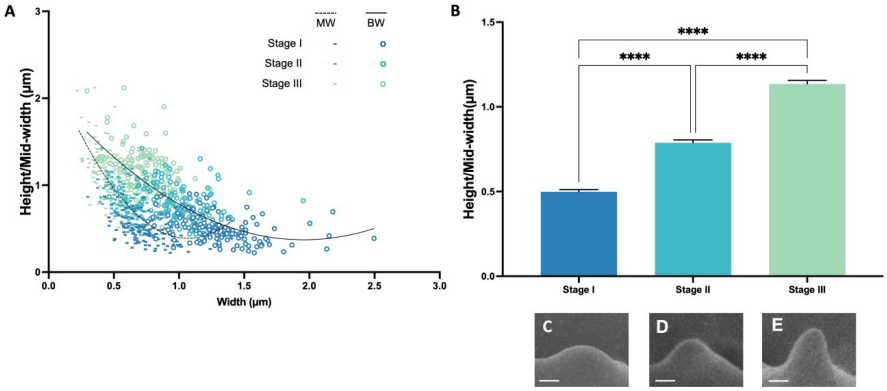

Figure 7: Dimensions of Spicules from FE-SEM micrographs. (A) Comparison of Height to Mid-width ratio versus width at the base (BW) and half-height (MW) for Stage I – III spicules. Quadratic best fit curve of the overall base width (solid black, r2=0.55) and mid width (dotted black, r2=0.59) overlain. (B) Average shape of RBC spicules, height to mid-width ratio, for stage I–III echinocytes. Kruskal Wallis with Dunn's multiple comparison, **Note:** ****p<0.0001. (C,D,E) Exemplars of spicules from SEM micrographs from stage I, II, and III echinocytes, respectively. Scale bars are 0.5µm. MW (-) Stage I; (-) Stage II; (-) Stage III; BW (∘) Stage I; (∘) Stage II; (∘) Stage III

Temperature, oxygen, and treatment also influence the spicule shape (as represented by the H/MW ratio) for all three stages of echinocytes, but the differences are most pronounced in stage I. Spicule shapes are plotted as best fit parabolas based on average dimensions of spicules in each condition (37˚C/10% O_2; 37˚C/0% O_2; 45˚C/10% O_2; 45˚C/0% O_2). In stage I, the spicules in hypoxic conditions result in narrower morphologies, and in hyperthermic condition at arterial oxygen levels, the stage I spicules are both shorter and narrower. Note that the general shape of the hyperthermic and physiologic temperature conditions are very similar, but the spicule is smaller. In stage II and stage III the aspect ratio for spicules are similar across all conditions, but we can see that hyperthermic condition at arterial oxygen results in consistently smaller spicules, and stage III spicules in physiologic arterial oxygen condition has the tallest spicule shape. When comparing stage I, II, and III spicule shapes in each condition, the stage I vs stage III shape is most pronounced in normal arterial conditions (Figures 8A-8D).

The H/MW ratio for stage I spicules in autologous plasma at physiologic temperature and arterial oxygen is 0.54 ± 0.06 (Figure 9A, black). Oxygen and temperature do not affect the spicule shape for stage I echinocytes in autologous plasma. PBS and PBS+1% DMSO do not alter spicule shape of stage I echinocytes compared to autologous plasma, regardless of temperature and oxygen (Figure 9A, black, red, orange). At 37˚C and 10% O_2, DIDS has significantly broader spicules than PBS+1% DMSO, whereas RBCs treated with Jasp and LatA form narrower and taller spicules (Figure 9A). Similarly, with heat, LatA promotes narrower spicules with oxygen depletion. Unlike arterial oxygen, in oxygen depletion, DIDS significantly increases the H/MW ratio. At high temperature and oxygen depletion, spicule shape is similar for RBCs in plasma alone, treated with DIDS, Jasp, and LatA, all of which have spicules which are approximately 2x wide as they are tall (Figure 9, yellow). CytoD creates shorter, broad spicules regardless of temperature and oxygen. In Stage II, we do not see the same effects of membrane disruptors (Figure 9B). In fact, Stage II shows no statistically significant differences among the spicule shape in the various treatment conditions. In Stage III, there are no statistically significant differences between controls and pharmacologic treatments. However, the largest difference in spicule shape appears in the DIDS treatment compared to CytoD for physiologic temperature and arterial oxygen (Figure 9C), in which DIDS produces tall, narrow spicules.

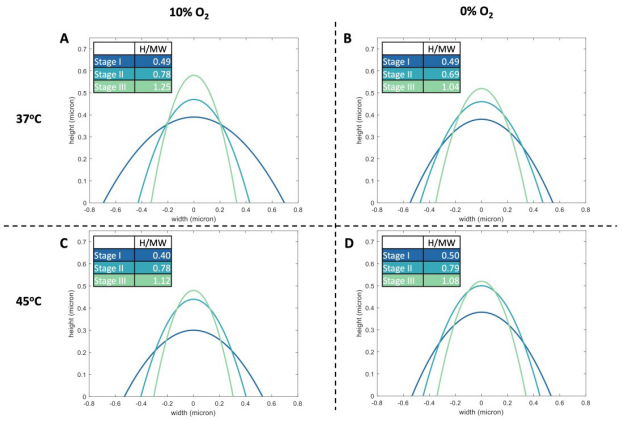

Figure 8: Spicule shape for stage I, II, and III echinocytes across temperature and oxygen saturation. Each chart illustrates the average spicule shape (based on height, base width, and mid width) for all measured spicules. Apex of each spicule is arbitrarily placed x=0 to show relative shape change. RBCs in all treatments exposed to typical physiologic temperature (37˚C) (A-B), arterial oxygen saturation (10 % O_2), (B,D) deoxygenated (0 % O_2), (A,C) and elevated temperature (45˚C) (C,D). Average values for height/mid-width ratio.

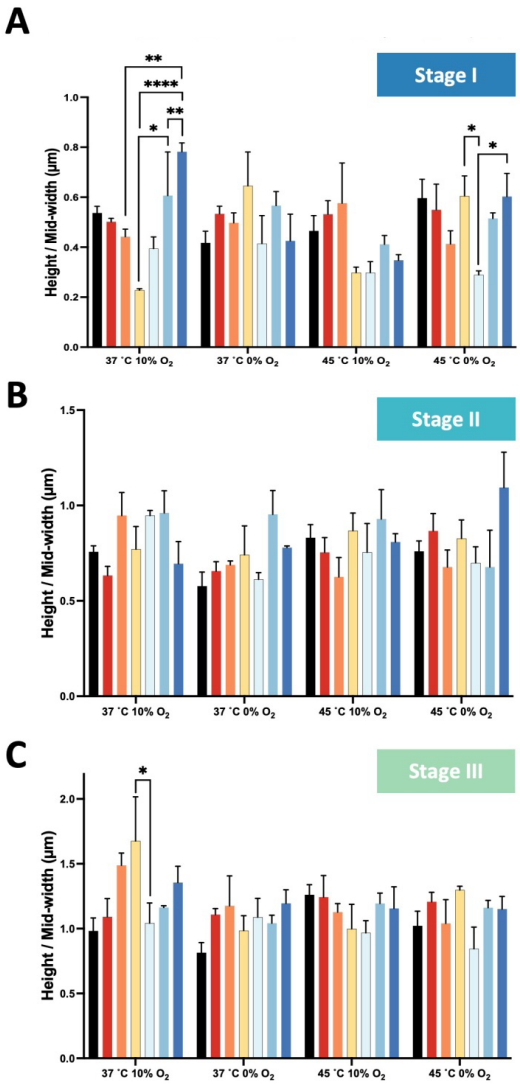

Figure 9: Shape of spicules from stage I-III echinocytes with membrane- or cytoskeleton-destabilizing treatments. Height to mid width ratio for stage I (A), II (B), and III (C) echinocytes in autologous plasma alone (■), PBS (■), PBS+1%DMSO (■), membrane destabilizer (DIDS,■), or actin disruptors, CytoD (■), Jasp (■) or LatA (■). RBCs in all treatments exposed to (from left to right) typical physiologic temperature and arterial oxygen saturation, hypoxemia, hyperthermia, and hypoxemia and hyperthermia. Bar graphs indicate mean height to mid width ratio, error bars indicate standard error of the mean. (2-way analysis of variance with Tukey's multiple comparisons test, *p<0.05, **<0.01, ****<0.0001 compared to other conditions at same temperature and oxygen saturation).

In addition to spicule shape, the arrangement of spicules on the echinocyte surface appears to display some degree of symmetry. It displays the average angle between adjacent spicules, regardless of treatment, temperature, and oxygen saturation (Figure 10A). The median angle for Stage I echinocytes is close to 5-fold symmetry, and the median angle for the Stage II and III echinocytes is between 6-fold and 7-fold symmetry. The angle between face spicules covers a wide ranges dependent on echinocyte stage, temperature, and oxygen. In arterial oxygen, for both 37˚C and 45˚C, we see a step-wise decrease in the angle between spicules from stage I through III echinocytes (Figure 10B). However, at 37˚C and 0% oxygen, this trend is no longer visible, and the spicule angle is consistently smaller. Notably, there are very few angles measured for stage I echinocytes, as stage I echinocytes are characterized by irregularity of edges, rather than spicules [20]. The median angle between spicules on stage II and III echinocytes at both 37˚C and 45˚C in arterial oxygen is 50˚–61˚ (Figure 10B). The median angle between spicules on stage II echinocytes at 37˚C in 0% O_2 is 67˚. The largest difference between stage I and stage III spicule angles is observed in the hyperthermic conditions. At 45˚C, regardless of oxygen saturation, the stage I echinocytes exhibit a lower packing density of spicules and the stage III echinocytes exhibit a higher packing density (lower angle arrangements).

There are no significant differences in packing density of spicules for stage I or II echinocytes (Figure 11). Notably, far fewer stage I echinocytes (n=8) were measured compared to Stage II (n=60) and Stage III (n=73), thus statistical comparisons for stage I echinocytes may be misleading. Regardless of temperature and oxygen, there are no differences for all echinocyte stages between autologous plasma, PBS, and PBS+1% DMSO (Figure 11). The variation in spicule angle across all treatment conditions shows that DIDS plays a large role in spicule angle for stage III comparisons at 10% O_2 conditions, but not in low oxygen conditions (Figure 11). At 45˚C, DIDS promotes high packing density, in which the mean angle between spicules is only 37.7˚, which approximates 9-10-fold symmetry. In physiologic temperature and arterial oxygen, Jasp produces a lower packing density for stage III echinocytes compared to all other treatments, and compared to stage II echinocytes (Figure 11A). Interestingly, there are no significant differences between treatments in the deoxygenated conditions (both 37 ˚C and 45˚C) (Figures 11B-11D).

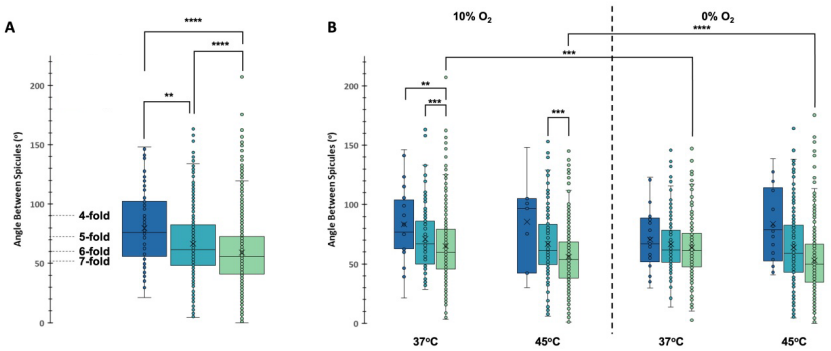

Figure 10: Angle between echinocyte face spicules from FE-SEM micrographs. (A) Angle between apex spicule and two nearest neighbor spicules for all echinocyte cells (stage I, II, and III) with perfect symmetry angles for 4-, 5-, 6-, and 7-fold symmetry are indicated, and (B) angle between apex spicule and two nearest neighbor spicules separated based on normal core temperature (37˚C) or elevated temperature (45˚C) and oxygen saturation (10 % O_2) or desaturation (0 % O_2). Box indicates upper and lower quartile, whiskers indicate range outside upper/lower quartile. Mean (×) and median (line) are shown for each box. Kruskal Wallis with Dunn's multiple comparison, **Note:** **p<0.01, ***<0.001, ****<0.0001. ((■) Stage I; (■) Stage II; (■) Stage III.

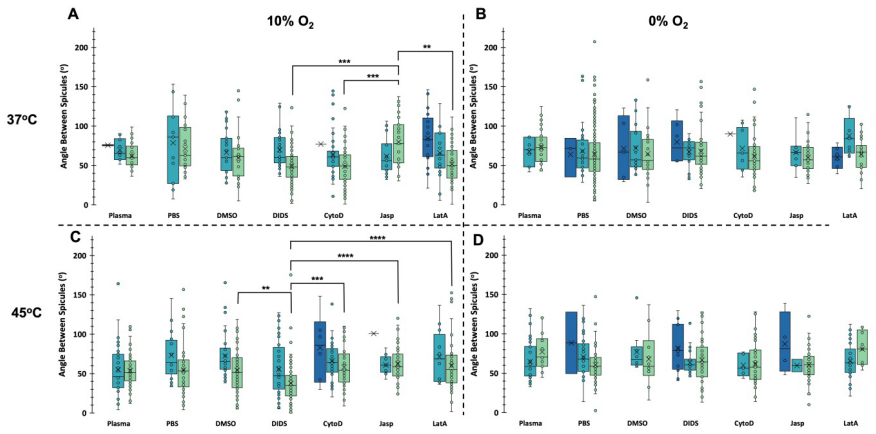

Figure 11: Angle between echinocyte face spicules with membrane- or cytoskeleton-destabilizing treatments. Angle between apex spicule and two nearest neighbor spicules on echinocytes in autologous plasma, PBS, PBS+1%DMSO, or with membrane destabilizer (DIDS) or actin disruptors (CytoD, Jasp, or LatA). All RBCs exposed to typical physiologic temperature (37˚C) (A-B), arterial oxygen saturation (10 % O_2), (B,D) deoxygenated (0 % O_2), (A,C) and elevated temperature (45˚C) (C,D). Box and whisker plots show quartile ranges for angle distributions. Far fewer stage I echinocytes were observed and measured (cells: n=18; spicule angles: n=66) compared to stage II (cells: n=60; spicule angles: n=600) and stage III (cells: n=73; spicule angles: n=1,644). (Kruskal Wallis with Dunn's multiple comparisons test, **Note:** **p<0.01, ***<0.001, ****<0.0001 compared to other conditions at same temperature and oxygen saturation for same stage of echinocyte). (■) Discocyte; (■) Stage I; (■) Stage II; (■) Stage III.

DISCUSSION

The key finding of this study is that while size, topology, and topography agree with the qualitative descriptions of stage I, II, and III echinocytes, within each stage, spicule morphology can differ depending on oxygen, temperature and type of cytoskeletal disruption. This implies that there are varying mechanisms by which spicules are produced.

For reference, Supplemental Figures 2-5 show schematic interpretation for cell size, spicule size, nearest neighbor distance, and spicule symmetry, along with a paired exemplar SEM micrograph. Stage III echinocytes are smaller and more spherical than their stage I and II counterparts. RBCs in plasma and treated with DIDS display six- to seven-fold symmetry, whereas RBCs treated with actin-disruptors display 5- to 6-fold symmetry. Interestingly, despite the morphology classification of stage III echinocytes, stage III echinocytes display various spicule symmetry, displays exemplar SEM images of stage III echinocytes displaying 6-fold, 7-fold, and 9-fold symmetry. Thus, the stage III morphology descriptor encompasses several more distinct morphologies within it, dependent on treatment (pharmacologic treatment, temperature, and oxygen) (Figures 12A-12C).

It is well known that RBCs are deformable, with many factors that can alter deformability, and thus influence cell shape [2-4]. Two of those factors, thermal stress and hypoxemia, are both associated with various pathological phenomena, i.e. thermal burn injury, stroke, myocardial infarction, and COVID-19 in which red blood cells are known to aggregate [47-50]. Prior literature has evaluated the morphology of heat treated RBCs, however the temperature range of focus was greater than that observed in pathologic states [51]. Further, it has been shown that RBCs are more deformable in an oxygenated environment compared to a deoxygenated environment, as is found in pathologic conditions [52].

The biconcave shape is mediated by components of the erythroid membrane in which, when altered, various abnormal RBC morphologies are produced. Thus, we examined the morphology of RBCs in physiologic (37˚C) and elevated (45˚C) temperatures and arterial (10%) and depleted (0%) oxygen. Temperature was shown to have a greater effect on morphology than oxygen, as there were more echinocytes present at elevated temperatures. This implies that temperature plays a larger role on deformability, perhaps through modulating the arrangement of cytoskeletal or membrane proteins.

Interestingly, all treatments, DIDS, CytoD, Jasp, and LatA, reduced the population of discocytes and shifted the population towards various stages of echinocytes. These changes were not independent of temperature and oxygen, however, as different treatments elicited different effects. Of note, DIDS shifted the population to stage III echinocytes for all temperatures and oxygens, except at high temperature and oxygen depletion, DIDS shifted the population to stage I echinocytes. DIDS is known to react with Lys-539 or Lys-542, which when bound significantly alters the ability for deoxy-hemoglobin (deoxyHb) to bind the N-terminal domain of band3 [26,43]. Thus, it is possible that with high temperature and oxygen depletion, DIDS and deoxyHb compete for binding, resulting in a more stable morphology of stage I echinocytes, as opposed to the more advanced stage III.

A potential limitation of the morphologic analysis is the use of brightfield microscopy, as the resolution was not optimal for identifying slight differences between cell morphologies; depending on the orientation of the cell in the field of view, discocytes and stage I echinocytes appeared similar. This is particularly noticeable for RBCs incubated in autologous plasma and PBS, where discocytes and stage I echinocytes, together, compose approximately 75% of the population of RBCs. Further, it is also possible that the pH decreased due to RBC suspensions warming to 37˚C or 45˚C, which could also drive the discocyte-echinocyte transformation.

While the population of morphologies of RBCs was dependent on temperature, oxygen, and treatment, it was unknown if the characteristics within those populations were similar. We thus evaluated the topology and topography of echinocyte spicules using SEM for the enhanced resolution, as compared to the clinical standard for evaluating morphology of brightfield microscopy [53]. Based on the qualitative descriptions made by Brecher and Bessis, the decreasing size of RBCs progressing from discocytes to stage I through III echinocytes is as expected [18]. It is also important to note that while the average size of discocytic RBCs is 7.5 µm-8.7 µm, it is expected that the fixation and serial dehydration process of sample preparation for SEM can cause some cell shrinkage [1,2,54]. To account for possible cell shrinkage, we prepared a sample using critical point drying and compared the RBC sizes obtained from SEM micrographs to those obtained *via* ethanol evaporation. There were no size differences observed in the two methods for SEM preparation.

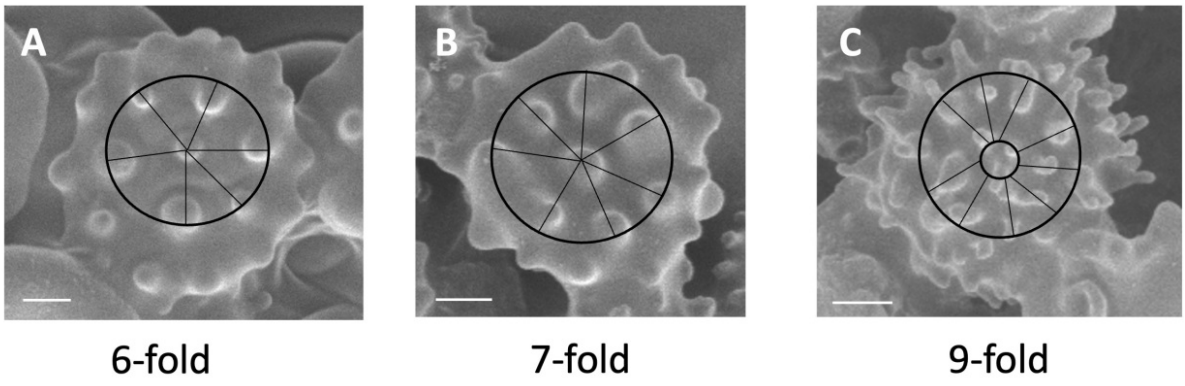

Figure 12: FE-SEM micrographs of stage III echinocytes with various spicule symmetry. Stage III echinocytes with (A) 6-fold symmetry (RBCs in PBS+1%DMSO at 45˚C 10 % O_2), (B) 7-fold symmetry (RBCs in DIDS at 37˚C at 10 % O_2), and (C) 9-fold symmetry (RBCs in DIDS at 45˚C at 10 % O_2). Black circle with lines overlain to trace over the central spicule(s) and surrounding spicules composing the symmetrical organization. Scale bars are 1 µm.

Brecher and Bessis describe stage I, II, and III echinocytes as an irregularly contoured disc, a flattened ellipse with rounded spicules, and a sphere with sharper spicules uniformly distributed over the surface, respectively [18]. The quantitative analysis of spicules thus agrees with their qualitative description, as stage I spicules have a base width as broad as one-fifth the diameter, and a low height to mid-width ratio, indicating a short, broad spicule. Stage I spicules have the greatest distance between their neighboring spicules, and have a very large angle between neighboring spicules, indicating that not many spicules are present. Despite our use of the term spicule when describing the bumps on stage I echinocytes, we question its appropriateness, as these bumps are better characterized as nodulations or irregular edges. Quantification of the morphological characteristics of spicules on stage II and III echinocytes also agree with the aforementioned descriptions, as stage III spicules have a base width about one-third the size of stage I and the largest height to mid-width ratio, indicating a taller, narrower spicule. Stage III spicules are the most closely packed, both shortest distance and smallest angle to nearest neighbors. Stage II spicules geometries lie directly between that of stage I and stage III.

The shape of stage II spicules did not differ between temperature, oxygen, and treatment, however, stage III spicules and stage I nodulations had various shapes (height to mid-width ratio). This too coincides with the descriptions of echinocytes, as stage I echinocytes are given the least precise definition and are simply identified by irregularity of edges. As is seen on the SEM micrograph inserts of Figure 7, the shape of stage I surface contours differs from broad nearly flat ridges on the surface, to the beginnings of a spicule, protruding from the surface of the cell. It is from these nodulations that the progressive stages of spicules form, until the spicule eventually buds off to form membrane vesiculations and the start of the stage IV echinocyte, also known as the spheroechinocyte [18]. The formation of the spheroechinocyte is proposed to occur when a fragile spicule, without cytoskeletal support, breaks off at the tip, causing microvesiculation [36]. However, this proposition conflicts with the composition of Extracellular Vesicles (EV), as they are heterogeneous, composed of band 3, actin, glycoproteins, membrane-associated proteins, negatively charged phospholipids, among others [38]. Thus, while the components of EVs hints at the potential composition of spicules, the two are not identical, and the ultimate budding mechanism is thus unknown. The presence of actin and other cytoskeletal proteins in EVs refutes the possibility that there is no cytoskeletal support. Instead, it suggests that dynamic actin reorganization destabilizes the junctional complexes that anchor the membrane to the cytoskeleton.

As the organization of the RBC membrane is well characterized [20], we looked at the spicule orientation to see if we could link the surface organization to the lattice meshwork beneath the surface. From stage I through stage III, spicule space filling goes from a median 76°, approximately five-fold symmetry with average 1.7 ± 0.5 μm nearest neighbor distance, to a more compact 56°, approximately six-fold symmetry with average 1.0 ± 0.3 μm nearest-neighbor distance. For stage III echinocytes, the actin disruptors, CytoD, Jasp, and LatA, all maintain a hexagonal spicule lattice topologic symmetry, as in plasma alone. Interestingly, 6 spectrin dimers bind per actin filament in a quasi-hexagonal unit cell, of 3500 nm^2. Within this unit cell, the actin filament is approximately 37nm long and tethered to 32 nm spectrin dimers [20,33,35]. Actin forms complexes with band 3, termed the actin junctional complex. Each actin junctional complex can either be associated with a single band 3 dimer or six band 3 dimers, encompassing 36 nm × 23 nm [20]. Nearest neighbor distances between spicules are 3 magnitudes larger than each actin junctional complex, which suggests that multiple of these hexagonal junctional complexes may be involved in forming echinocyte spicules. Thus, the formation of spicules likely occurs at a junction point that enmeshes multiple actin junctional complexes, accounting for the contribution of both band 3 and actin.

CONCLUSION

Overall, actin-disruptors, CytoD, Jasp, and LatA, appeared to have less of an effect on spicule morphology than DIDS, an agent with a specific uncoupling effect between the membrane and cytoskeleton. DIDS binds band 3 adjacent to the location that band 3 interacts with ankyrin, thereby connecting the membrane to the actin cytoskeleton. This suggests that rather than band 3 or actin contributing to echinocyte and spicule formation, it is the interaction between band 3, ankyrin, spectrin, and actin, that promotes the energetically favorable shape of the RBC. When this connection is altered or severed, by DIDS binding band 3, or a change in actin polymerization state, the RBC adopts a new energetically favorable state, shifting towards echinocyte. Our results aid in further understanding of the mechanism of spicule formation. Further studies should evaluate the composition of RBC spicules throughout the stage I-III echinocytes.

DECLARATION

Conflict of interest

The authors declare that the research was conducted in the absence of any commercial or financial relationships that could be construed as a potential conflict of interest.

Author contributions

S. Weber-Fishkin, L.D. Frame, and M. D. Frame conceived the study. S. Weber-Fishkin and M.D. Frame prepared all samples. S. Weber-Fishkin obtained brightfield micrographs. L.D. Frame obtained SEM micrographs. All authors conceived the method for image analysis. A. Eligulashvili and L.D. Frame analyzed all SEM images. S. Weber-Fishkin and M.D. Frame analyzed and interpreted the results. S. Weber-Fishkin wrote the manuscript under the guidance of M.D. Frame, her dissertation advisor. Portions of the study will be published in S. Weber-Fishkin's Ph.D. thesis. All authors have seen and approved of the final version of the manuscript being submitted.

Funding

American Association of University Women (AAUW) Dissertation Fellowship (S. Weber-Fishkin). UCONN School of Engineering Interdisciplinary Multi-Investigator Materials Proposals award (L. Frame).

Acknowledgments

We thank Alexander Perkins and Sebastian Kopilak for contributing to SEM data acquisition.

Data availability statement

The raw data supporting the conclusions of this article will be made available by the authors, without undue reservation.

REFERENCES

1. Diez-silva M, Dao M, Han J, Lim CT, Suresh S. Shape and biomechanical characteristics of human red blood cells in health and disease. MRS Bull. 2010; 35:382-388.
2. Litvinov RL, Weisel JW. Role of red blood cells in haemostasis and thrombosis. Isbt Sci Ser. 2017; 12: 176-183.

3. Kim JLh, Shin S. Advances in the measurement of red blood cell deformability: A brief review. J Cell Bitech. 2015; 1:63-79.

4. Loebl EC, Baxter CR, Curreri PW. The mechanism of erythrocyte destruction in the early post-burn period. Ann Surg. 1973; 178:681-6.

5. Ivanov IT, Paarvanova B, Slavov T. Dipole relaxation in erythrocyte membrane: Involvement of spectrin skeleton. Bioelectrochemistry. 2012; 88:148-55.

6. Lim HJ, Lee YJ, Nam JH, Chung S, Shin S. Temperature-dependent threshold shear stress of red blood cell aggregation. J Biomech. 2010; 43: 546-50.

7. Faber CGTJ, Vermes I, Lodder J, Kalsbeek-Batenburg EM, Kessels F, Haanen C. Enhanced red blood cell aggregation unrelated to fibrinogen: A possible stroke mechanism in young patients. Cerebrovasc Dis. 1997; 7: 70-76.

8. Beamer N, Giraud G, Clark W, Wynn M, Coull B. Diabetes, hypertension and erythrocyte aggregaton in acute stroke. Cerebrovasc Dis. 1997; 7:144-149.

9. Takeshita SKH, Toriuchi K, Aoki H, Ueda H, Wakatsuki A, Yamada Y, et al. Impact of covid-19 on red blood cell rheology. Br J Haematol. 2021;192:99-120.

10. Lanier ST, Mcclain SA, Lin F, Singer AJ, Clark RA. Spatiotemporal progression of cell death in the zone of ischemia surrounding burns. Wound Repair Regen. 2011; 19: 622-32.

11. Munoz S, Sebastian JL, Sancho M, Alvarez G. Elastic energy of the discocyte-stomatocyte transformation. Biochim Biophys Acta. 2014; 1838:950-956.

12. Bull BS, Brailsford JD. The biconcavity of the red cell: An analysis of several hypotheses. Blood. 1973; 41: 833-844.

13. Uzoigwe C. The human erythrocyte has developed the biconcave disc shape to optimise the flow properties of the blood in the large vessels. Med Hypotheses. 2006; 67: 1159-1163.

14. Smith AS, Nowak RB, Zhou S, Giannetto M, Gokhin DS, Papoin J, et al. Myosin iia interacts with the spectrin-actin membrane skeleton to control red blood cell membrane curvature and deformability. Proc Natl Acad Sci USA. 2018; 115:4377-4385.

15. Cooper RA, Durocher JR, Leslie MH. Decreased fluidity of red cell membrane lipids in abetalipoproteinemia. J Clin Invest. 1977; 60:115-121.

16. Mentzer WC. Causes of spiculated cells (echinocytes and acanthocytes) and target cells. UpToDate.2017

17. Strohm EM, Berndl ES, Kolios MC. Probing red blood cell morphology using high-frequency photoacoustics. Biophys J. 2013; 105: 59-67.

18. Brecher G, Bessis M. Present status of spiculed red cells and their relationship to the discocyte-echinocyte transformation: A critical review. Blood. 1972; 40:333-344.

19. Gokhin DS, Fowler VM. Feisty filaments: actin dynamics in the red blood cell membrane skeleton. Curr Opin Hematol. 2016; 23:206-214.

20. Lux SE. Anatomy of the red cell membrane skeleton: Unanswered questions. Blood. 2016; 127: 187-199.

21. Luna EJ, Hitt AL. Cytoskeleton-plasma membrane interactions. Science. 1991; 258: 955-964.

22. Rasia M, Bollini A. Red blood cell shape as a function of medium's ionic strength and pH. Biochim Biophys Acta. 1998; 1372:198-204.

23. Butler J, Mohandas N, Waugh RE. Integral protein linkage and the bilayer-skeletal separation energy in red blood cells. Biophys J. 2008; 95:1826-1836.

24. Nehls V, Zeitler-Zapf P, Drenckhahn D. Different sequences of expression of band 3, spectrin, and ankyrin during normal erythropoiesis and erythroleukemia. Am J Pathol. 1993; 142: 1565-1573.

25. Lombardo CR, Willardson BM, Low PS. Localization of the protein 4.1-binding site on the cytoplasmic domain of erythrocyte membrane band 3. J Biol Chem. 1992; 267:9540-9546.

26. Chu H, Breite A, Ciraolo P, Franco RS, Low PS. Characterization of the deoxyhemoglobin binding site on human erythrocyte band 3: Implications for O_2 regulation of erythrocyte properties. Blood. 2008; 111: 932-938.

27. Chu H, Mckenna MM, Krump NA, Zheng S, Mendelsohn L, Thein SL, et al. Reversible binding of hemoglobin to band 3 constitutes the molecular switch that mediates O_2 regulation of erythrocyte properties. Blood. 2016; 128: 2708-2716.

28. Melzak KA, Moreno-Flores S, Bieback K. Spicule movement on RBCs during echinocyte formation and possible segregation in the RBC membrane. Biochim Biophys Acta Biomembr. 2020; 1862 (10): 183338.

29. Iglic A. A possible mechanism determining the stability of spiculated red blood cells. J Biomech. 1997; 30: 35-40.

30. Kruger-Genge AJF, Kupper JH, Lehmann C, Franke RP. Actin type and distribution in erythrocytes. J Cell. Biotechnol. 2018; 3: 81-83.

31. Spector I, Braet F, Shochet NR, Bubb MR. New anti-actin drugs in the study of the organization and function of the actin cytoskeleton. Microsc Res Tech. 1999; 47: 18-37.

32. Picart C, Discher DE. Actin protofilament orientation at the erythrocyte membrane. Biophys J. 1999; 77: 865-78.

33. Gokhin DS, Nowak RB, Khoory JA, Piedra ade L, Ghiran IC, Fowler VM. Dynamic actin filaments control the mechanical behavior of the human red blood cell membrane. Mol Biol Cell. 2015; 26: 1699-710.

34. Mohandas N, Gallagher PG. Red cell membrane: Past, present, and future. Blood. 2008; 112: 3939-48.

35. Fowler VM. The human erythrocyte plasma membrane: A Rosetta Stone for decoding membrane-cytoskeleton structure. Curr Top Membr. 2013; 72:39-88.

36. Mukhopadhyay R, Lim HWG, Wortis M. Echinocyte shapes: Bending, stretching, and shear determine spicule shape and spacing. Biophys J. 2002; 82:1756-72.

37. Franke RP, Scharnweber T, Fuhrmann R, Wenzel F, Kruger A, Mrowietz C, et al. Effect of radiographic contrast media on the spectrin/band3-network of the membrane skeleton of erythrocytes. PLoS One. 2014; 9: 89512.

38. Thangaraju K, Neerukonda SN, Katneni U, Buehler PW. Extracellular Vesicles from Red Blood Cells and Their Evolving Roles in Health, Coagulopathy and Therapy. Int J Mol Sci. 2020; 22(1):153.

39. Barbarino F, Waschenbach L, Cavalho-Lemos V, Dillenberge RM, Becker K, Gohlke H, et al. Targeting spectrin redox switches to regulate the mechanoproperties of red blood cells. Biol Chem. 2021; 402(3): 317-331.

40. Sorensen PM, Iacob RE, Fritzsche M, Engen JR, Brieher WM, Charras G, et al. The natural product cucurbitacin E inhibits depolymerization of actin filaments. ACS Chem Biol. 2012. 7(9): 1502-1508.

41. Cooper JA. Effects of cytochalasin and phalloidin on actin. J Cell Biol. 1987; 105(4): 1473-1478.

42. Lepke S, Fasold H, Pring M, Passow H. A study of the relationship between inhibition of anion exchange and binding to the red blood cell membrane of 4,4'-diisothiocyano stilbene-2,2'-disulfonic acid (DIDS) and its dihydro derivative (H_2DIDS). J Membr Biol. 1976; 29: 147-177.

43. Janas TJ. Reversible DIDS binding to band 3 protein in human erythrocyte membranes. Mol Membr Biol. 2000; 17(2): 109-115.

44. van Dort HM, Knowles DW, Chasis JA, Lee G, Mohandas N, Low PS. Analysis of integral membrane protein contributions to the deformability and stability of the human erythrocyte membrane. J Biol Chem. 2001; 276(50): 46968-46974.

45. Schindelin J, Arganda-Carreras I, Frise E, Kaynig V, Longair M, Pietzsch T, et al. Fiji: an open-source platform for biological-image analysis. Nat Methods. 2012; 9(7): 676-682.

46. Schneider CA, Rasband WS, Eliceiri KW. NIH Image to ImageJ: 25 years of image analysis. Nat Methods. 2012; 9(7): 671-675.

47. Levin GY, Egorihina MN. Aggregation of erythrocytes in burn disease. Int J Burns Trauma. 2011; 1(1):34-41.

48. Baskurt OKM, Herbert J. Role of red blood cell aggregation in tissue perfusion: New findings. Sang Throm Vais. 2010; 22: 137-143.

49. Pretorius E, Lipinski B. Thromboembolic ischemic stroke changes red blood cell morphology. Cardiovasc Pathol. 2013; 22: 241-242.

50. Gerard D, Ben Brahim S, Lesesve JF, Perrin J. Are mushroom-shaped erythrocytes an indicator of COVID-19? Br J Haematol. 2021; 192: 230.

51. Repin NV, Bobrova EN, Repina SV. Thermally induced transformation of mammalian red blood cells during hyperthermia. Bioelectrochemistry. 2008; 73: 101-105.

52. Uyuklu M, Meiselman HJ, Baskurt OK. Effect of hemoglobin oxygenation level on red blood cell deformability and aggregation parameters. Clin Hemorheol Microcirc. 2009; 41: 179-188.

53. Ford J. Red blood cell morphology. Int J Lab Hematol. 2013; 35: 351-357.

54. Zhang Y, Huang T, Jorgens DM, Nickerson A, Lin LJ, Pelz J, et al. Quantitating morphological changes in biological samples during scanning electron microscopy sample preparation with correlative super-resolution microscopy. PLoS One. 2017; 12: 0176839.